

G-type antiferromagnetic structure in the metallic d-wave altermagnet $Rb_{1-\delta}V_2Te_2O$

Wu Xie(谢武), Changchao Liu(刘长超), Fayuan Zhang(张发远), Zhenhong Tan(谭振宏), Wenhai Ji(季文海), Nan Zhao(赵南), Lingxiang Bao(鲍伶香), Dong Zhang(张栋), Feiran Shen(沈斐然), Hao Wang(王浩), Rong Du(杜蓉), Lunhua He(何伦华), Guanghan Cao(曹光旱), Chaoyu Chen(陈朝宇), and Ping Miao(缪平)

Citation: Chin. Phys. B, 2026, 35 (**8**): 087503. DOI: 10.1088/1674-1056/ae8f1a
http://cpb.iphy.ac.cn; http://iopscience.iop.org/cpb

What follows is a list of articles you may be interested in

Higher-order topological semimetal induced by altermagnet

Dengfeng Wang(王登凤), Xiang Ji(吉祥), and Sen Cui(崔森)
Chin. Phys. B, 2026, 35 (**7**): 077510. DOI: 10.1088/1674-1056/ae6b35

Multiferroicity and thermal expansion of the layered metal-organic framework $[NH_4Cl]_2[Ni(HCOO)_2(NH_3)_2]$

Dan Cheng(程丹), Yingjie He(何英杰), Shuang Liu(刘爽), Na Su(苏娜), and Young Sun(孙阳)
Chin. Phys. B, 2025, 34 (**6**): 067505. DOI: 10.1088/1674-1056/adcaa4

Alternating spin splitting of electronic and magnon bands in two-dimensional altermagnetic materials

Qian Wang(王乾), Da-Wei Wu(邬大为), Guang-Hua Guo(郭光华), Meng-Qiu Long(龙孟秋), and Yun-Peng Wang(王云鹏)
Chin. Phys. B, 2024, 33 (**9**): 097507. DOI: 10.1088/1674-1056/ad6425

Incommensurate-commensurate magnetic phase transition in double tungstate $Li_2Co(WO_4)_2$

Xiyu Chen(陈西煜), Ning Ding(丁宁), Meifeng Liu(刘美风), Tao Zou(邹涛), V. Ovidiu Garlea, Jingwen Gong(龚婧雯), Fei Liu(刘飞), Yunlong Xie(谢云龙), Lun Yang(杨伦), Shuhan Zheng(郑书翰), Xiuzhang Wang(王秀章), Shuai Dong(董帅), T. Charlton, and Jun-Ming Liu(刘俊明)
Chin. Phys. B, 2022, 31 (**4**): 047501. DOI: 10.1088/1674-1056/ac3818

The magnetic properties and magnetocaloric effects in binary *R*-*T* (*R*=Pr, Gd, Tb, Dy, Ho, Er, Tm; *T*=Ga, Ni, Co, Cu) intermetallic compounds

Xin-Qi Zheng(郑新奇), Bao-Gen Shen(沈保根)
Chin. Phys. B, 2017, 26 (**2**): 027501. DOI: 10.1088/1674-1056/26/2/027501

RAPID COMMUNICATION

G-type antiferromagnetic structure in the metallic d-wave altermagnet $Rb_{1-\delta}V_2Te_2O$

Wu Xie(谢武)[1,2], Changchao Liu(刘长超)[3], Fayuan Zhang(张发远)[4], Zhenhong Tan(谭振宏)[1,2], Wenhai Ji(季文海)[1,2], Nan Zhao(赵南)[1,2], Lingxiang Bao(鲍伶香)[1,2], Dong Zhang(张栋)[1,2], Feiran Shen(沈斐然)[1,2], Hao Wang(王浩)[1,2], Rong Du(杜蓉)[1,2], Lunhua He(何伦华)[1,5], Guanghan Cao(曹光旱)[3,†], Chaoyu Chen(陈朝宇)[6,‡], and Ping Miao(缪平)[1,2,§]

[1] *Spallation Neutron Source Science Center, Dongguan* 523803, *China*
[2] *Institute of High Energy Physics, Chinese Academy of Sciences, Beijing* 100049, *China*
[3] *School of Physics, Zhejiang University, Hangzhou* 310058, *China*
[4] *Quantum Science Center of Guangdong–Hong Kong–Macao Greater Bay Area, Shenzhen* 518045, *China*
[5] *Beijing National Laboratory for Condensed Matter Physics, Institute of Physics, Chinese Academy of Sciences, Beijing* 100190, *China*
[6] *Songshan Lake Materials Laboratory, Dongguan* 523803, *China*

(Received 20 July 2026; revised manuscript received 22 July 2026; accepted manuscript online 23 July 2026)

Altermagnetism, known for its non-relativistic spin-split band structures with yet compensated moments, is being intensively investigated. Discovering new altermagnetic materials with characteristics suitable for practical use remains an important ongoing task. Recently, a metallic room-temperature altermagnet candidate $Rb_{1-\delta}V_2Te_2O$ with a layered structure and d-wave spin symmetry has been reported based on experimental results from spin-resolved photoemission spectroscopy and scanning tunnelling microscopy/spectroscopy measurements. Here we report neutron powder diffraction investigations on the magnetic structure of $Rb_{1-\delta}V_2Te_2O$, which show a G-type antiferromagnetic structure below the transition temperature of 337 K. The result is different from the original theoretical expectation, which might lead to new insights on the physics of this altermagnet candidate.

Keywords: altermagnetism, neutron powder diffraction

PACS: 75.50.Ee

DOI: 10.1088/1674-1056/ae8f1a **CSTR:** 32038.14.CPB.ae8f1a

1. Introduction

Altermagnetism represents one of the typical unconventional mechanisms for realizing spin-polarized electronic states, in addition to the Rashba–Dresselhaus effect arising from the spin–orbit coupling (SOC) in compounds with inversion symmetry breaking, and Zeeman-type spin splitting in ferromagnets with time-reversal symmetry breaking. While extensive theoretical and experimental efforts have led to the discovery of a series of altermagnets with typical characteristics,[1–11] this field is confronting controversies on specific candidates.[12–14] Exploring new altermagnetic materials with favorable properties for practical use remains an important ongoing task.

Recently a metallic room-temperature altermagnet candidate $Rb_{1-\delta}V_2Te_2O$ has been reported, which features a layered structure and exhibits spin polarization of d-wave symmetry.[10] Such d-wave symmetric spin splitting is favorable for generating non-relativistic spin currents, meanwhile the layered structure facilitates the exfoliation from bulk into thin films and the integration with other materials in spintronic device fabrications. With its high transition temperature above room temperature, $Rb_{1-\delta}V_2Te_2O$ serves as one of the most promising altermagntic material platforms for both fundamental research and applications in spintronics and valleytronics devices.

Experimentally, although the angle-resolved photoemission spectroscopy (ARPES) and scanning tunnelling microscopy/spectroscopy (STM/STS) measurements[10] show opposite spin splitting between crystal-symmetry-paired valleys and suppression of intervalley scattering as a consequence of the spin–valley locking, respectively, investigations on the microscopic magnetic structure in $Rb_{1-\delta}V_2Te_2O$ have not been reported. The calculations based on density functional theory (DFT) have predicted a ground state of C-type antiferromagnetic (AFM) structure, whose energy is only around 1 meV/supercell lower than the G-type AFM structure in $Rb_{1-\delta}V_2Te_2O$, as shown in Fig. 1.[15] Very recently, in the sister compound $Cs_{1-\delta}V_2Te_2O$, a G-type AFM structure has been confirmed based on neutron diffraction investi-

†Corresponding author. E-mail: ghcao@zju.edu.cn
‡Corresponding author. E-mail: chenchaoyu@sslab.org.cn
§Corresponding author. E-mail: miaoping@ihep.ac.cn

© 2026 Chinese Physical Society and IOP Publishing Ltd. All rights, including for text and data mining, AI training, and similar technologies, are reserved.

gations, where similar spin polarization has been observed on the spin-resolved ARPES measurements.[16] The concepts of "hidden altermagnetism" and local altermagnetic order were adopted to reconcile the obtained magnetic structure and the spin slittings in momentum space,[16] as proposed earlier by theorists.[17] Since G-type AFM structure favors altermagnetism only in a single sector in-plane while C-type AFM structure is favorable for altermagnetism as a whole, it is rather important to pin down the microscopic magnetic structure in $Rb_{1-\delta}V_2Te_2O$, which imposes strong constraints on the interpretation of the observed d-wave symmetric spin polarization.

As shown in Fig. 1, both G-type and C-type AFM exhibit an in-plane Néel-type antiparallel configuration and differ only in the alignment between adjacent layers. In $Rb_{1-\delta}V_2Te_2$ and other compounds in the 1221-family with a quasi-2D layered structure, the interlayer magnetic coupling is weak, which leads to a tiny energy difference between the G-type and C-type AFM ground states. The small interlayer coupling renders the underlying magnetic structure susceptible to small perturbations, such as deficiency and/or self-doping effects, etc., which may vary in different batches of samples. On the other hand, it is difficult for the DFT calculations to capture every detail of a real material. Actually, the DFT calculations on the 1221-compounds from different groups have led to contradictory results. For instance, a G-type AFM structure has also been reported as a magnetic ground state for $Rb_{1-\delta}V_2Te_2$.[18] For CsV_2Te_2O, DFT calculations show that the C-type AFM is more stable at $U = 0$ (U is the onsite Coulomb interaction), while for $U \geq 1$eV, G-type AFM is the magnetic ground state.[19] Therefore, complete and detailed experimental investigations are really necessary to determine the magnetic structure in $Rb_{1-\delta}V_2Te_2O$.

In this work, we report detailed neutron powder diffraction (NPD) investigations on the magnetic structure of $Rb_{1-\delta}V_2Te_2O$ ($0.12 \leq \delta \leq 0.18$). Pure magnetic peaks indexed by a magnetic propagation vector of (0, 0, 0.5) were observed below the Néel temperature T_N of 337 K, while no magnetic peak featuring the C-type AFM structure was observed. Moreover, Rietveld refinements using the FullProf software suite unambiguously point to a G-type AFM structure in $Rb_{1-\delta}V_2Te_2O$.

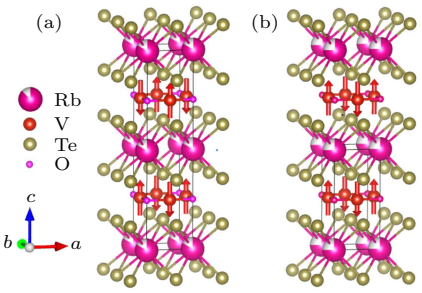


Fig. 1. The illustration of two typical magnetic structures of $Rb_{1-\delta}V_2Te_2O$. The G-type and C-type AFM structures are displayed in panel (a) and (b), respectively.

2. Experimental methods

Polycrystals of $Rb_{1-\delta}V_2Te_2O$ were synthesized via a solid-state reaction method, as reported in Ref. [18]. The as-prepared sample was characterized by powder x-ray diffraction (XRD) at room temperature using a PANalytical diffractometer (Empyrean Series 2) with monochromatic Cu-$K_{\alpha 1}$ radiation. A minor impurity phase of V_2O_3 less than 5 % was determined from XRD. Magnetic susceptibility was measured on a Quantum Design physical property measurement system (QD-PPMS) using a vibrating sample magnetometer (VSM) insertion. In total, three batches of polycrystalline samples were prepared for neutron experiments.

Neutron powder diffraction (NPD) measurements were conducted at the time-of-flight high-resolution neutron diffractometer (TREND) and the general-purpose powder diffractometer (GPPD) at the China Spallation Neutron Source (CSNS).[20–23] The well-ground powder sample was loaded into a 10 mm VNi holder under a helium atmosphere and sealed via indium wire. The sample was mounted in a cryofurnace, and the NPD data were collected at temperatures ranging from 5 K to 350 K, across the Néel temperature. Due to the air- and water-sensitivity of the sample, all experimental operations related to the sample were conducted under inert gases. One batch of sample was measured at GPPD, and the other two batches were measured at TREND.

The Rietveld refinements of neutron data were performed using the FullProf software suite,[24] where the K_{SEARCH} program was used for determining the magnetic propagation vector (k-vector), and BasIreps was adopted for the irreducible representation (Irreps) analysis during the magnetic model construction. In addition, programs on the Bilbao Crystallographic Server (https://www.cryst.ehu.es), in particular MAXMAGN and k-SUBGROUPSMAG, were adopted to identify the maximal magnetic space groups.[25] Finally, VESTA was utilized for structure visualization and presentation.[26]

3. Results and discussion

The polycrystalline sample for neutron study was firstly checked with magnetic susceptibility $\chi(T)$ measurement. As shown in Fig. 2, two transitions have been observed: the magnetic transition T_N at 337 K and the metal-to-metal transition T^* at 116 K. The two transitions are both higher than those reported in literature,[10,18] which are most likely due to the sample dependence, such as the slightly different Rb-occupancy.

Figure 3 shows the FullProf refinement results of powder neutron diffraction data of $Rb_{1-\delta}V_2Te_2O$ above and below T_N. As shown in Fig. 3(a), for $T = 350$ K, a crystal structure model of $Rb_{1-\delta}V_2Te_2O$ with space group (SG) $P4/mmm$ (No. 123) is adopted for the refinement, together with the high temperature phase of V_2O_3 (SG: R-3c) as a known impurity phase. Besides, there is at least one more impurity peak as

indicated by asterisks in Fig. 3(a). The peaks from impurity phases show negligible temperature dependence down to 5 K. The refined crystal structure for $Rb_{1-\delta}V_2Te_2O$ is consistent with that reported in literature.[18] The obtained Rb vacancy δ is between 0.12 and 0.18 for three different batches of samples of $Rb_{1-\delta}V_2Te_2O$.

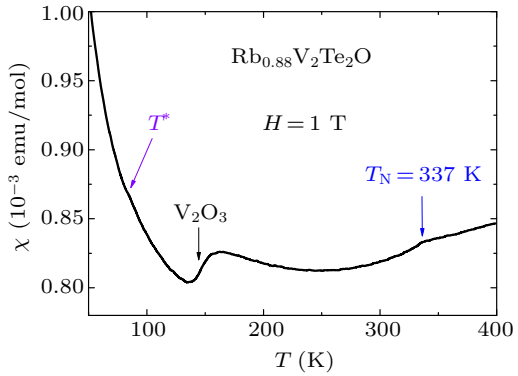


Fig. 2. Magnetic susceptibility χ versus T of $Rb_{1-\delta}V_2Te_2O$ polycrystal under a magnetic field of 1 T, where the positions of two transitions T_N and T^* are noted by the blue and purple arrows, respectively. The drop at around 150 K is related to the structural transition of V_2O_3.

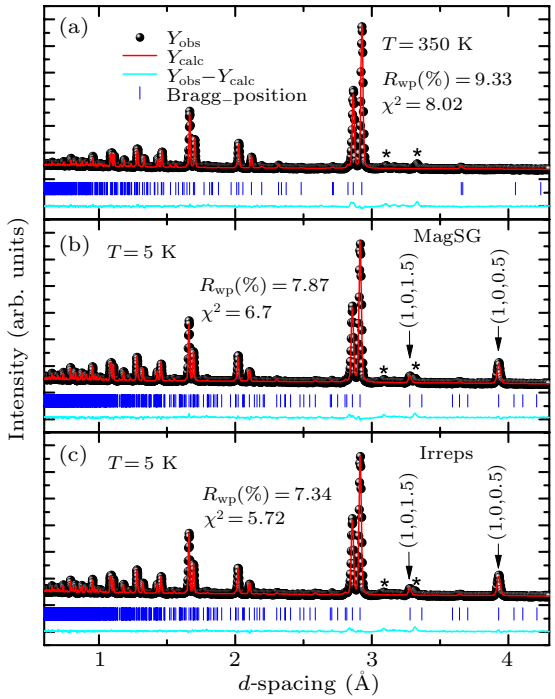


Fig. 3. The results of Rietveld refinements of the NPD data obtained from TREND at (a) T = 350 K, and (b), (c) T = 5 K, respectively. Panels (b) and (c) show the 5 K data fitted with the magnetic phase modeled using two different methodologies, respectively, which result in the same G-type AFM structure. The asterisks denote the peaks from a minor impurity phase, while the black arrows in panels (b) and (c) indicate the positions of two strong magnetic peaks.

Upon cooling, two additional peaks are observed as denoted by the arrows in Figs. 3(b) and 3(c). Using K_{SEARCH}, a k-vector of (0, 0, 0.5) is undoubtedly determined, and the two magnetic peaks can be indexed as (1, 0, 0.5) and (1, 0, 1.5), respectively. The G-type AFM and C-type AFM structures as shown in Fig. 1 are indexed by different magnetic propagation vectors: (0, 0, 0.5) for G-type, and (0, 0, 1) for C-type. Consequently, the G-type AFM structure will generate additional reflections (magnetic peaks) below the Néel temperature T_N, while for the C-type AFM structure, the magnetic peaks all appear on top of the nuclear peaks. Therefore, the observation of additional magnetic peaks rules out the possibility of the C-type AFM structure.

Table 1. The G-type antiferromagnetic structure of $Rb_{1-\delta}V_2Te_2O$ is described under its magnetic space group (MagSG, crystallographic description), with basic information about its relation to its parent paramagnetic structure. All items in the table are supported by the magnetic CIF format (mcif).

Items	Details
Compound	$Rb_{1-\delta}V_2Te_2O$
Parent space group	$P4/mmm$ (No.123)
Propagation vector(s)	(0, 0, 0.5)
Basis transformation from parent basis	$(a, b, 2c;\ 0, 0, 0)$
MagSG symbol (number)	P_c4_2/mcm (132.456)
Basis transformation to standard setting of MagSG	$(a, b, c;\ 0, 0, 1/4)$
Unit cell parameters (Å)	$a = 4.03813(8)$ $b = 4.03724(16)$ $c = 16.8181(4)$ $\alpha = 90.0000$ $\beta = 90.0000$ $\gamma = 90.0000$
MagSG symmetry operations	1 $x, y, z, +1$ 2 $-x, -y, -z, -1$ 3 $y, -x, z, -1$ 4 $y, x, -z, -1$ 5 $-y, -x, z, +1$ 6 $-x, y, z, -1$ 7 $y, x, z, +1$ 8 $x, -y, z, -1$ 9 $x, y, -z, -1$ 10 $-y, x, z, -1$ 11 $-y, -x, -z, -1$ 12 $y, -x, -z, +1$ 13 $x, -y, -z, +1$ 14 $-x, y, -z, +1$ 15 $-x, -y, z, +1$ 16 $-y, x, -z, +1$
MagSG symmetry centering operations	1 $x, y, z, +1$ 2 $x, y, z+1/2, -1$
Positions of atoms	Te1 0.50000 0.50000 0.13539 V1 0.00000 0.50000 0.25000 O1 0.00000 0.00000 0.25000 Rb1 0.00000 0.00000 0.00000
Magnetic moment (μ_B) of magnetic atoms, symmetry constraints and moment magnitudes at 5 K	V1 0.00000 0.00000 1.425(13) (0, 0, m_z) 1.425(13)

Below T_N, a magnetic model is further considered in the FullProf refinement through two methodologies: magnetic space group (MagSG) and irreducible representation (Irreps). The maximal magnetic space groups compatible with a k-vector of (0, 0, 0.5) are analyzed using MAX-

MAGN on the Bilbao Crystallographic Server. While in total 12 maximal magnetic space groups are listed, only four among them allow nonzero magnetic moments for the V-ions: P_c4_2/mcm (#132.456), P_c4/mcc (#124.360), C_cmcm (#63.466) and P_amma (#51.298). Among them, P_c4_2/mcm and P_c4/mcc correspond to G-type and A-type AFM structures, respectively, with moments along the c-axis, while the moments are constrained in the ab-plane for C_cmcm and P_amma. We have tested all four magnetic models in FullProf refinements and finally concluded that the G-type AFM model of magnetic space group P_c4_2/mcm (#132.456) gives the best fit to the magnetic peaks, as shown in Fig. 3(b). As for the representation analysis, three Irreps are obtained: i.e., Γ_2 of one dimension, Γ_4 of one dimension, and $2\Gamma_9$ of two dimensions ($1\Gamma_2+1\Gamma_4+2\Gamma_9$), which correspond to G-type AFM, A-type AFM, and in-plane noncollinear AFM structures, respectively. The Rietveld refinement also indicates that the G-type AFM model of Γ_2 fits best to the pattern as shown in Fig. 3(c), consistent with the results from the MagSG methodology. The obtained V-moment sizes at 5 K are 1.425(13) μ_B from MagSG and 1.449(12) μ_B from Irreps, respectively. The basic information of the obtained G-type AFM structure of $Rb_{1-\delta}V_2Te_2O$, described under its MagSG, is listed in Table 1. Note that the impurity phase V_2O_3 undergoes a first-order structural transition at $\sim$ 170 K.[27] Therefore, for the refinements below 170 K, the low-temperature phase of V_2O_3 (SG: $C2/c$) is included in the Rietveld refinement.

Rietveld refinements were performed on all three batches of polycrystalline samples measured at two different neutron diffractometers, TREND and GPPD, at CSNS. The results show that the magnetic ground state remains a G-type AFM structure despite the Rb vacancy varying from 0.12 to 0.18. We also notice that samples with larger Rb occupancy (less vacancy) tend to have a higher transition temperature T_N, indicating a more stable magnetic state. Therefore, the magnetic ground state of the perfect crystal without Rb-vacancy might remain the G-type antiferromagnetic structure.

The G-type AFM structure will largely renew the explanation of the previously reported spin-ARPES data. Unlike C-type AFM, the spin-opposite sublattices of the G-type AFM structure can be connected by translation or inversion operations, which is not consistent with a d-wave spin splitting observed in the electronic structure. On the other hand, analogous to that in locally noncentrosymmetric compounds with local spin polarizations, a G-type AFM could support local altermagnetism in a single sector along the c-axis,[18] which has been proposed and termed as "hidden altermagnetism" or "compensated altermagnetism".[16,17] The concept of "hidden altermagnetism" could reasonably reconcile the present neutron diffraction results with the previously reported spin-ARPES data. So far, the experimentally confirmed "hidden altermagnetism" examples are still rare. Our results render $Rb_{1-\delta}V_2Te_2O$ as another candidate for "hidden altermagnetism".

Figure 4(a) shows the temperature dependence of the two magnetic peaks, whose intensities increase as temperature decreases. The temperature dependence of the magnetic moment size obtained from Rietveld refinements on data at each temperature is plotted in Fig. 4(b). An empirical formula $M = M_0(1-T/T_N)^\beta$ is adopted to fit the temperature dependence of the ordered moments as shown in Fig. 4(b), where M_0 is the ordered moment at zero temperature and β is the critical exponent. The obtained β value is 0.25±0.007. Note for two batches of polycrystalline samples with slightly different Rb vacancy, the reduced value of β is robust. One can therefore conclude that such a reduced critical exponent is not due to an effect of vacancy. In the sister compound KV_2Te_2O,[29] β was fitted to be about 0.48±0.02, where the magnetic moments were derived from the temperature dependent magnetic peak intensity via scaling. The discrepancy on the β value might arise from intrinsic difference between $Rb_{1-\delta}V_2Te_2O$ and KV_2Te_2O.

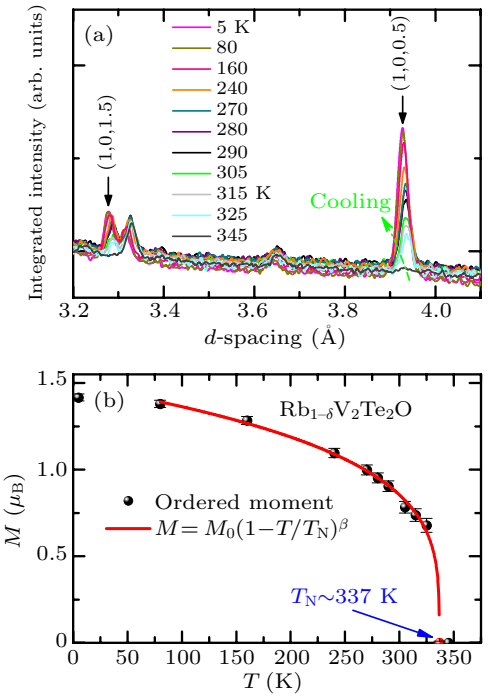


Fig. 4. (a) NPD data obtained from TREND in a selected d-range measured at a series of temperatures, showing the temperature dependent magnetic peak intensity. (b) Temperature dependence of the ordered moment. The red solid line is the fitted result as described in the main text. The red point is the transition point obtained from the temperature dependent magnetic susceptibility measurement.

The obtained β of $\sim$0.25 in $Rb_{1-\delta}V_2Te_2O$ is much smaller than that from a mean-field theory prediction ($\beta = 0.5$[30]), indicating a transition beyond the mean-field paradigm. Note that for a 2D-Ising model, β is reduced to 0.125,[31] and for a 3D-Ising model, β is about 0.326.[32] The observed β of 0.25 sits in between, which is possibly related to

a dimension-crossover effect, i.e., quasi-2D nature. Theoretically, a special critical point known as the tricritical-Lifshitz point with unusual critical exponents has been reported to exist in d-wave altermagnetic metals when altermagnetism coexists with superconductivity.[33] The physical mechanism underlying the reduced critical exponent observed here in a demonstrated d-wave altermagnetic metal remains an open question.

4. Summary

In summary, we have performed comprehensive NPD investigations on the metallic d-wave altermagnet candidate $Rb_{1-\delta}V_2Te_2O$, and a G-type AFM structure with moments along the *c*-axis has been determined to be the magnetic ground state. The result is different from the original expectation, where a C-type AFM structure is expected to support a global d-wave altermagnetism. Potential origins of the discrepancies are discussed. Since ARPES and STM data have revealed concrete experimental evidence for the d-wave spin symmetry, analogous to the recent report for $Cs_{1-\delta}V_2Te_2O$,[16] a hidden altermagnetism with alternating local spin polarization arising from a single stacking layer of the G-type AFM structure might act as a proper scenario to reconcile all experimental discoveries.

Acknowledgements

This work is supported by the National Key R&D Program of China (Grant Nos. 2023YFE0105700 and 2023YFA1406101), the National Natural Science Foundation of China (Grant Nos. 12304183, 12574068, and 12504185), Guangdong Innovative & Entrepreneurial Research Team Program (Grant No. 2021ZT09C539), and the Guangdong Basic and Applied Basic Research Foundation (Grant Nos. 2023B0303000003, 2023B1515120060, 2024B1515120045, and 2025B1515120034). The authors also acknowledge the neutron beam time at TREND (Shenzhen Guangming Science City Development and Construction Co., Ltd. and its Material Genome Big-Science Facilities Platform, https://cstr.cn/31113.02.CSNS.TREND) and General Purpose Powder Diffractometer (GPPD) (https://csns.cn/31113.02.CSNS.GPPD) at the China Spallation Neutron Source (CSNS) (https://cstr.cn/31113.02.CSNS). The authors also thank Dr. Wanju Luo for his assistance in the experiment.

References

[1] Šmejkal L, González-Hernández R, Jungwirth T and Sinova J 2020 Sci. Adv. **6** eaaz8809
[2] Ma H Y, Hu M, Li N, Liu J, Yao W, Jia J F and Liu J 2021 *Nat. Commun.* **12** 2846
[3] González-Hernández R, Šmejkal L, Výborný K, Yahagi Y, Sinova J, Jungwirth T and Železný J 2021 *Phys. Rev. Lett.* **126** 127701
[4] Smejkal L, Sinova J and Jungwirth T 2022 *Phys. Rev. X* **12** 031042
[5] Feng Z, Zhou X, Šmejkal L, Wu L, Zhu Z, Guo H, González-Hernández R, Wang X, Yan H, Qin P, Zhang X, Wu H, Chen H, Meng Z, Liu L, Xia Z, Sinova J, Jungwirth T and Liu Z 2022 *Nat. Electron.* **5** 735
[6] Bai H, Han L, Feng X Y, Zhou Y J, Su R X, Wang Q, Liao L Y, Zhu W X, Chen X Z, Pan F, Fan X L and Song C 2022 *Phys. Rev. Lett.* **128** 197202
[7] Krempaský J, Šmejkal L, D'Souza S W, *et al*. 2024 *Nature* **626** 517
[8] Amin O J, Dal Din A, Golias E, *et al*. 2024 *Nature* **636** 348
[9] Jiang B, Hu M, Bai J, *et al*. 2025 *Nat. Phys.* **21** 754
[10] Zhang F, Cheng X, Yin Z, *et al*. 2025 *Nat. Phys.* **21** 760
[11] Wu K, Dong J, Zhu M, Zheng F and Zhang J 2025 *Chin. Phys. Lett.* **42** 070702
[12] Song C, Bai H, Zhou Z, Han L, Reichlová H, Dil J H, Liu J, Chen X and Pan F 2025 *Nat. Rev. Mater.* **10** 473
[13] Jungwirth T, Sinova J, Fernandes R M, Liu Q, Watanabe H, Murakami S, Nakatsuji S and Šmejkal L 2026 *Nature* **649** 837
[14] Zhang X, Liu J, Huang W, Zhang F, Zhu M Y, Zhu Y P, Chen C, Liu C, Kim C and Shen D 2026 *Chin. Phys. Lett.* **43** 050709
[15] Supplementary information in Ref. [10]
[16] Yang G, Chen R, Liu C, *et al*. 2025 arXiv: 2512.00972
[17] Guo S D 2026 *Front. Phys.* **21** 025201
[18] Ablimit A, Sun Y L, Jiang H, Wu S Q, Liu Y B and Cao G H 2018 *Phys. Rev. B* **97** 214517
[19] Liu C C, Li J, Liu J Y, Lu J Y, Li H X, Liu Y and Cao G H 2025 *Phys. Rev. B* **112** 224439
[20] Tan Z, Li Z, Zhang D, Ma J, Xie W, Ji W, Wu Y, Kamiyama T and Miao P 2026 *Nucl. Instrum. Methods Phys. Res. A* **1083** 171096
[21] Wu Y, Xie W, Ma J, Zhang D, Cheng H, Tan Z, Ji W, Yin Y and Miao P 2025 *Instrum. Sci. Technol.* **54**
[22] Ma J, Ji W, Yu D, Tan Z, Xie W, Wu Y, Yu Y, Li Z, Wang T, Ke Z, Yin W, Wang Y, Kamiyama T and Miao P 2025 *Rev. Sci. Instrum.* **96** 063305
[23] Zhong J, Zhang D, Wang H, Tan Z, Xie W, Ji W, Li Y, Guo H, Miao P, Zhang J and Du R 2026 *Nucl. Instrum. Methods Phys. Res. A* **1082** 170928
[24] Rodr íguez-Carvajal J 1993 *Phys. B* **192** 55
[25] Gallego S V, Tasci E S, de la Flor G, Pérez-Mato J M and Aroyo M I 2012 *J. Appl. Crystallogr.* **45** 1236
[26] Momma K and Izumi F 2011 *J. Appl. Crystallogr.* **44** 1272
[27] Yethiraj M 1990 *J. Solid State Chem.* **88** 53
[28] Zhang X, Liu Q, Luo J W, Freeman A J and Zunger A 2014 *Nat. Phys.* **10** 387
[29] Sun Y, Huang Y, Cheng J, Zhang S, Li Z, Luo H, Ma X, Yang W, Yang J, Chen D, Sun K, Gutmann M, Capelli S C, Shen F, Hao J, He L, Chen G and Li S 2025 *Phys. Rev. B* **112** 184416
[30] Landau L D and Lifshitz E M 1980 *Statistical Physics*, Part 1 (3rd edn.)
[31] Yang C N 1952 *Phys. Rev.* **85** 808
[32] Guida R and Zinn-Justin J 1998 *J. Phys. A: Math. Gen.* **31** 8103
[33] Hu H and Liu X 2025 *AAPPS Bull.* **35** 35